Fatigue strength of longitudinal load-carrying welds in beams made of ultra-high-strength steel

Skriko Tuomas, Lipiäinen Kalle, Ahola Antti, Mettänen Heli, Björk Timo

Please cite the publication as follows:

T. Skriko, K. Lipiäinen, A. Ahola, H. Mettänen, T. Björk (2021) Fatigue strength of longitudinal load-carrying welds in beams made of ultra-high-strength steel, Journal of Constructional Steel Research, 179, 106563. DOI: 10.1016/j.jcsr.2021.106563

Fatigue strength of longitudinal load-carrying welds in beams made of ultra-high-strength steel

Tuomas Skriko[1], Kalle Lipiäinen[2], Antti Ahola[2*], Heli Mettänen[2], Timo Björk[2]

[1]Laboratory of Welding Technology, Lappeenranta-Lahti University of Technology LUT, P.O. Box 20, FI-53851, Lappeenranta, Finland

[2]Laboratory of Steel Structures, Lappeenranta-Lahti University of Technology LUT, P.O. Box 20, FI-53851, Lappeenranta, Finland

Abstract

The present study experimentally investigates the fatigue strength of longitudinally loaded welded joints in beam structures made of ultra-high-strength steel. Hereby, the effects of different manufacturing methods and welding preparations on the fatigue strength and the crack initiation locations of welded box and I section beams are evaluated. Specifically, experimental fatigue tests are carried out on welded these beams prepared with manual and automatic welding, and subjected to a constant amplitude four-point bending with an applied stress ratio of $R = 0.1$. The results show a variation in fatigue strength, whereby high performance is achieved using both single- and double-sided welds, particularly if the longitudinally continuous weld penetration is controlled by sufficient support of the weld root face. Current fatigue design codes and guidelines are applicable, albeit with some conservatism, for assessing the fatigue strength of longitudinal load-carrying welded joints made of ultra-high-strength steel.

1 Introduction

The use of high- and ultra-high-strength steels (HSS/UHSS) in demanding industrial applications has increased over the past decades. Typical UHSS structures in the field are load handling machines, vehicles, and lifting equipment such as telescopic booms and cranes. The aim is to reduce the weight of the structure, thereby increasing energy efficiency, or enable enhanced lifting or transportation payload capacities. The use of HSS and UHSS materials enables a reduction in the cross-sectional area [1], leading to thinner plate thicknesses compared to structures made of mild steels (e.g., S355). However, the slenderness of UHSS plate members increases the

*Corresponding author: antti.ahola@lut.fi (A. Ahola)

risk of instability issues, such as a buckling of the plate members [2] or a lateral buckling of the whole construction. The avoidance of local buckling phenomena leads to geometrically more complicated cross sections, which together with thinner plate thicknesses are prone to additional stresses due to the distortion of cross section. Both design and manufacturing factors become significant when reaching high fatigue properties because the processing and handling (e.g., forming and machining) of UHSSs is more demanding; welding, in particular, has a stricter parametric window in which to operate compared to low-strength steel grades [3–5].

In addition to the challenges and requirements related to static loads and manufacturing, the consideration of fatigue performance is of paramount importance when welded UHSS structures are introduced for structural applications. Prior investigations [6,7] have univocally shown that material strength does not necessarily contribute to high fatigue strength in welded components in the as-welded condition. Meanwhile, the use of UHSS components targets an increase in stress levels, including fatigue load actions. Post-weld treatment (PWT) techniques, such as grinding [8], TIG dressing [9], and high frequency mechanical impact (HFMI) treatment [10,11], as well as weaving techniques during welding [12] are efficient means to improve the fatigue strength of welded UHSS joints, as long as the load conditions, and weld sizing and penetration can prevent fatigue failures originating from the weld root [13]. However, these improvement methods cannot be purposefully utilized for longitudinal load-carrying welds because the fatigue strength is unaffected by the notch quality at the weld toe in the perpendicular direction. Instead, it is substantially affected by the longitudinal geometry of the weld root or toe.

Prior investigations concerning the fatigue behavior of welded HSS and UHSS materials tended to focus on transversely loaded joints (see e.g., [14–18]), and they only had a limited scope on large-scale components, such as tubular joints and connections (see e.g., [19,20]). Nevertheless, with PWTs [9,10] and a good design practice of joints, e.g., by positioning transverse joints in low-stress areas, the fatigue strength of longitudinal weldments in beam components and girders might become critical and, hence, an important fatigue design criterion [21,22]. Feldmann et al. [23] and Bartsch et al. [24] re-evaluated the detail categories of the EC3 standard [25], including longitudinal weldments, with respect to early fatigue test data (from the 1960s and 1970s). They found a good agreement between the test data and current design recommendations (see also Section 2.2 for further details of the fatigue strength assessments of longitudinal load-carrying weldments). The collected experimental data also incorporated the results from Fisher et al. [26] that showed no beneficial effect on fatigue strength when the material strength was increased (up to the yield strength of 700 MPa). Böhme et al. [27] evaluated the effect of pores on the fatigue performance of longitudinal T-joint welds finding pores as critical for fatigue crack

initiation but their size did not have significant effect on the fatigue strength capacity. Recently, Hanji et al. [28] fatigue-tested low-strength (yield strength f_y = 317–341 MPa) steel I-beam girders, fabricated using gas metal arc welding (GMAW) and laser-arc hybrid welding, under four-point bending; they observed equal or even higher fatigue strengths for the laser-arc hybrid-welded joints compared to the GMA-welded joints. Nevertheless, these studies principally focused on low-strength steel materials, and further studies on the fatigue behavior of longitudinal welds in UHSS materials are required.

The aim of the present study is to experimentally investigate the fatigue strength of longitudinal weldments in UHSS grade welded I and box section beams in comparison with the current fatigue design recommendations [25,29–31]. A total number of 19 large-scale beam structures (8 box sections and 11 I section specimens) were fatigue-tested under four-point bending loading with an applied stress ratio of $R = 0.1$. The groove preparation (double-beveled, single-beveled, and fillet) and weld type (single-sided and double-sided), and the welding process (GMAW and laser) were altered to investigate their effects on the weld geometry, location of fatigue crack nucleation, and fatigue strength in longitudinal weldments.

2 Fatigue strength of longitudinal welds

2.1 General design aspects of longitudinally loaded welded joints in beam structures

In beam structures, welded joints connect parallel metal sheets and bars to obtain a desired structure and cross-section form under bending and torsional moment loads, as demonstrated in Fig. 1a. Such longitudinal welds ensure that a cross section acts as a fixed profile – without the longitudinal welds, individual sheet components slide relative to each other when beam structures are loaded; hence, the stiffness of unwelded beams remains much lower compared to welded ones. Typically, shear forces acting on weldments are low to moderate and, therefore, rather small throat thicknesses of fillet welds are needed according to the static strength criterion [32].
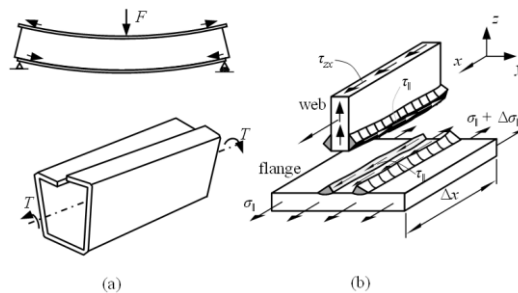

Fig. 1. (a) Principles and requirements for longitudinal welds under bending and torsional moments, and (b) stresses at the longitudinal fillet welds of an I-beam subjected to bending, according to Niemi [33].

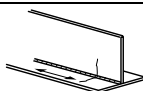*Corresponding author: antti.ahola@lut.fi (A. Ahola)

The stresses acting on a welded joint of a bending-loaded beam structure are illustrated in Fig. 1b. Preventing the sliding phenomenon described above by means of welds, results in longitudinal shear stresses (τ_l) at the welds, which are primary stresses affecting them. In addition, the axial stresses of the beam are shown as longitudinal normal stresses (σ_l) in the welds although these are secondary stresses in terms of joint functionality in regard to the weldments.

The design criteria for longitudinally loaded welded joints in beam structures depends on the load actions, i.e. whether a structure will be subjected to predominantly static or cyclic and fluctuating loads. In statically loaded joints, fillet welds or bevel groove welds, without the need for full penetration, are generally appropriate. However, for structures subjected to cyclic loads, several different factors need to be taken into account to achieve a high quality in welded joints and, thus, high fatigue resistance. These factors are addressed in detail in Section 2.2.

2.2 Fatigue strength assessment of longitudinal load-carrying welds

In the design codes and guidelines for the fatigue strength assessment of welded joints [25,29–31], longitudinal welds subjected to parallel normal stress (load-carrying) are categorized based on the weld type (fillet weld or K-butt weld), presence of welding start and stop positions (with or without), and level of welding automation (robotic/mechanized or manual). Table 1 summarizes the characteristic design fatigue classes as per the manufacturing process for longitudinal welds in web-to-flange connections.

Table 1. Characteristic fatigue classes for continuous longitudinal welds in the web-to-flange connections of box and I sections.

Welded detail	Description	Fatigue class [MPa]			
		EC3 [25]	IIW [30]	DNV-GL [29]	EN 13001[*] [31]
	Automatic fully penetrated K-butt welds without start/stop positions	125	125	125 (C)	–
	Automatic fillet welds (both sides) without start/stop positions	125	112	125 (C)	180
	Automatic fillet welds (both sides) containing start/stop positions	125	–	112 (C1)	140
	Automatic fillet weld (one-sided) containing start/stop positions	112	–	–	–
	Manual longitudinal fillet or butt weld	100	90	100 (C2)	–

[*]In accordance with the EN ISO 5817 standard [34], quality levels B and C for FAT180 and FAT140, respectively. In addition, the requirements of +1 NC (notch class) in the case of no irregularities from the start/stop positions in weld quality level C and -1 NC for welding with a restrained shrinkage, are met [31].

[*]Corresponding author: antti.ahola@lut.fi (A. Ahola)

In longitudinal load-carrying welds, to achieve a high fatigue resistance, the weld toe and root side geometry should have a continuous shape in the longitudinal direction without any discrepancies. Thus, while the weld toe radius and flank angle do not play a significant role, as they do in transversely loaded weldments, the longitudinal continuity resulting from both the travel and movement of the welding torch, and potentially from the start/stop positions is of paramount importance. Hence, the automatized or robotized welds have a higher fatigue strength than manually welded joints in the design codes and guidelines [25,29,30].

In welded beam structures a with closed-formed cross section, such as box sections, longitudinal welds are normally prepared only from one side due to the inaccessibility to inside a closed-form structure, and the weld root fatigue becomes thus a critical detail despite the loading direction. In longitudinally loaded welds, the control of penetration is essential, and it is difficult to manage without a backing plate. Two illustrative weld root shape are exemplified in Fig. 2. If a full penetration weld without a backing plate is applied, the weld root geometry becomes non-uniform in the longitudinal direction (Fig. 3a) which decrease fatigue strength. Alternatively, a weld with the partial penetration has a better weld root continuity, but it leaves a non-fused root face which can act as an initial crack (Fig. 3b) for transverse load actions. This raises the need for the careful consideration of the joint and weld configuration in longitudinally loaded welded joints subjected to fatigue loading.
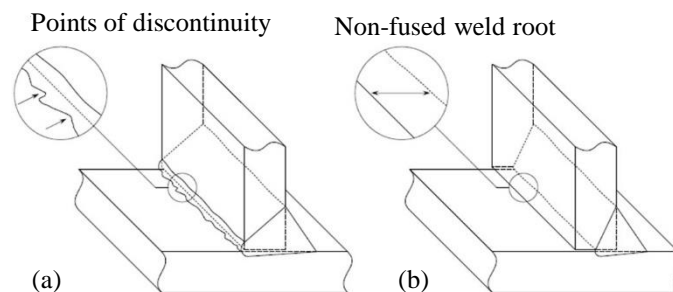
Fig. 2. Weld root geometries for (a) fully penetrated, and (b) partially penetrated web-to-flange connections with a single-sided weld in accordance with [35].

In addition to the welding procedure itself and the quality at the weld root (the control of the weld penetration), different welding preparation factors with respect to structural factors, e.g., plate thicknesses, should also be taken into account in terms of longitudinal continuity of the joint. The locations of tack welds have to be considered because they can affect the welding penetration and, consequently, produce major points of discontinuities [28]. In addition, if welds with partial penetration are used, a fatigue strength assessment for cut edges should be conducted due to possible micro-cracking of the steel plate face, associated with the high tensile residual stress in

*Corresponding author: antti.ahola@lut.fi (A. Ahola)

the longitudinal direction. Under fluctuating load conditions, the fatigue crack can propagate from these initial flaws if the cut surface remains non-fused. Machined edges also enable a uniform contact or root gap between welded plates and thus, a uniform penetration form without any longitudinal discontinuities. In [36], S460M T-profile specimens with double-sided fillet welds were longitudinally fatigue tested and an equal number of fatigue failures initiated from the oxy-fuel cut edge and weld area.

3 Experiments

3.1 Materials

The base material used in this study was S960 MC structural steel, which is a low-alloyed structural steel that has a dual-phase microstructure comprising martensite and bainite [37]. The applied filler metal was a Böhler Union X96 solid wire; although this nominally an undermatching filler material compared to the base material but, practically, the Union X96 weld metal has similar or even higher ultimate strength properties than the S960 MC base material [38,39], and it is widely used in the welding of UHSSs.

In addition to the above-mentioned materials, 20 mm thick S355 flat bars were used in the top flanges (under compression, see Fig. 3b and 7a) in manufacturing the test specimens. The thicker S355 material was chosen to avoid failures from the compression flange. Thicker plate thicknesses were not available in the studied S960 MC grade (t = 3–10 mm), and thus a low-strength structural steel had to be applied for the top flanges in most of the studied cases. The nominal chemical compositions and mechanical properties of the used base materials and filler metal are presented in Table 2 and Table 3, respectively.

Table 2. Nominal chemical compositions [wt-%] of the base materials and filler metal [40–42].

	C	Si	Mn	P	S	Al	Nb	V	Ti	Cu
Base materials										
S960 MC	0.12	0.25	1.30	0.020	0.010	0.015	0.050	0.050	0.070	
S355	0.20	0.55	1.60	0.025	0.025					0.55
	C	Si	Mn	Cr	Ni	Mo				
Filler metal										
Union X96	0.12	0.80	1.90	0.45	2.35	0.55				

Table 3. Nominal mechanical properties of the base materials and filler metal (minimum values) [40–42].

Material ID	Yield strength f_y [MPa]	Ultimate tensile strength f_u [MPa]	Elongation A_5 [%]	Impact strength T [°C]	KV [J]
Base materials					

*Corresponding author: antti.ahola@lut.fi (A. Ahola)

S960 MC	960	980–1250	7	-40	27
S355	345	470–630	20	-20	27
Filler metal					
Union X96	930	980	14	-50	47

3.2 Test specimens

Fatigue tests were performed on the beam structures using two different cross-section types of box sections (single- and double-symmetric), and an I-beam section. The geometries and dimensions of the cross-sections are presented in Fig. 3. The first three fatigue tests (specimens FF1-FF3) of the box sections were carried out using a double-symmetric geometry (Fig. 3a). With such a geometry, fatigue cracks initiate near the contacts of the four-point bending press rolls due to a thin top flange. This fatigue behavior was prevented by applying fully penetrating welds (throat thickness 9-10 mm) at the top flange-to-web connections near the press rolls. Moreover, the decision was made to alter the cross-section geometry of the box section specimens in the later fatigue tests (specimens FF4-FF8). With a single-symmetric box section (Fig. 3b), the location of the neutral axis in the vertically rose, and thus, the absolute bending stress at the bottom flange was higher than at the top flange. This enabled the crack initiation to occur in the studied joint areas, namely the bottom flange-to-web connections.

The I section specimens were designed in accordance with the findings from the fatigue tests on the box sections, and thus single-symmetric cross-sections were applied. In addition, buckling failure modes were taken into account in the design of the specimens (cross sections were class 3 [43]).
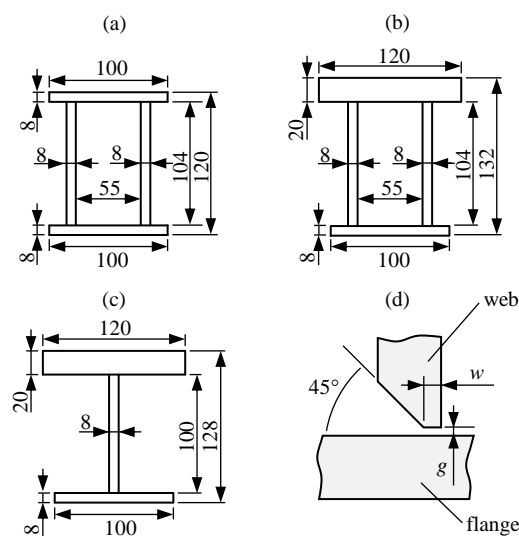
Fig 3. Cross-section shape and dimensions of the box section specimens (a) FF1-FF3 and (b) FF4-FF8, and (c) the I section specimens for the experimental fatigue tests; (d) groove dimensions (*w* is the width of root face and *g* is the air gap).

*Corresponding author: antti.ahola@lut.fi (A. Ahola)

The longitudinal welds of the box sections were single-sided, and thus, the weld root geometry of weld was a key factor in terms of fatigue performance. As it was not possible to confirm the full penetration at the weld root, partially penetrated welds were used for these specimens. Both gas metal arc welding (GMAW) and fiber laser welding were used to prepare box sections. Fig. 4 presents the macrographs of the different weld configurations. A nominal throat thickness of 4 mm was used to weld the box sections using GMAW. The applied welding parameters are presented in Appendix A (Table A.1).
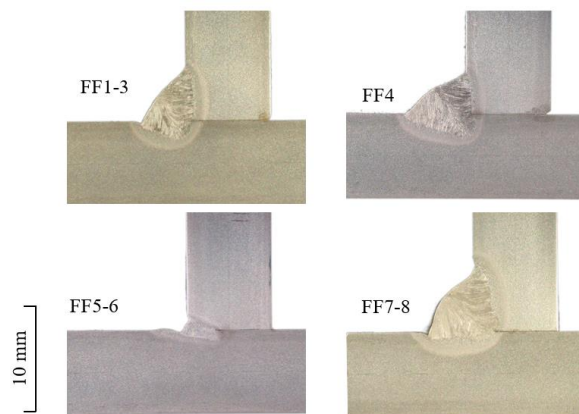
Fig. 4. Macrographs of the web-to-flange connections in the hollow section specimens.

In the grooved I section welds, the bevel angle was set to 45°, but the root face and gap varied between 0–1.0 mm and 0–3.0 mm, respectively, to attain different penetration depths. Three reference beams were welded double-sided with full penetration (K-butt). The macrographs of the I-beam bottom flange welds are presented in Fig. 5. The I-10 specimen was prepared a single bevel and welded from one side but as shown in Fig. 5, resulted in break-outs. Table 4 presents weld configurations applied in the I section specimens. The weld quality was assessed in accordance with the EN ISO 5817 standard [34], and the results are summarized in Table 6 for the imperfection categories relevant to the weldments used in this study.

Table 4. I section welding configurations.

ID	w [mm]	g [mm]	Beads/side	Weld type/groove
I-1, I-2, I-3	0	0	1	K-butt
I-4	8 (= t)	0	1	Single-sided fillet
I-5	1	0	1	Single bevel
I-6	1	0	2	Single bevel
I-7	0	2	2	Single bevel
I-8	0	3	2	Single bevel

*Corresponding author: antti.ahola@lut.fi (A. Ahola)

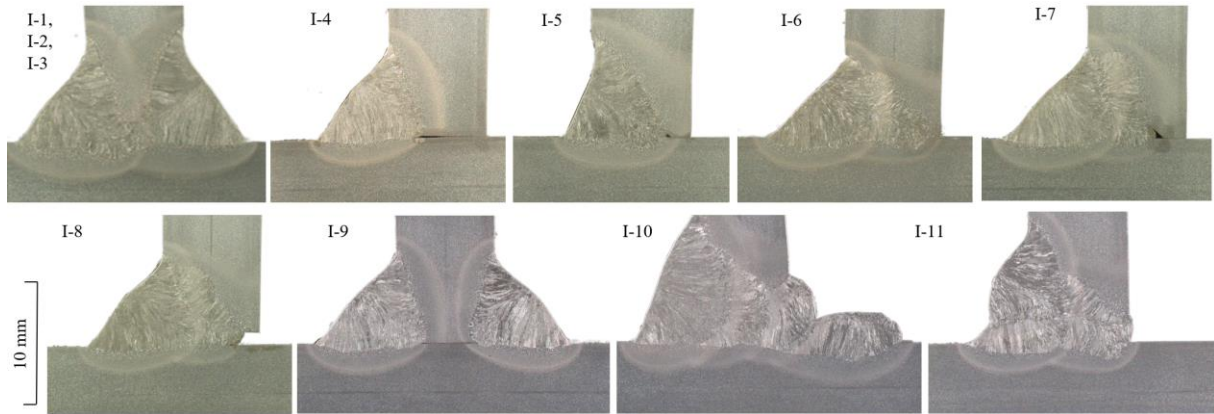| I-9 | 8 (= t) | 0 | 1 | Double-sided fillet |
| I-10 | 0 | 3 | 4 | Single bevel |
| I-11 | 0 | 1 | 3 | Single bevel |

Fig. 5. Macrographs of the web-to-flange connections in the I section specimens.

Table 5. Evaluated weld imperfections and quality levels (B to D) of the tested specimens in accordance with the EN ISO 5817 standard [34], see also Fig. 4 and Fig. 5 for comparisons. Only the imperfections relevant to this study are presented.

Specimen ID	EN ISO 5817 imperfections			
	1.7 Intermittent undercut	1.10 Excessive convexity	1.11 Excess penetration	1.16 Excessive asymmetry
FF1–3	B	B	B	B
FF4	B	B	B	B
FF5–6	n/a [a]	n/a [a]	B	n/a [a]
FF7–8	C	B	B	B
I-1, I-2, I-3	B	B	B	B
I-4	B	B	B	B
I-5	B	B	B	n/a [a]
I-6	B	B	B	B
I-7	B	B	B	B
I-8	B	B	B	B
I-9	B	B	B	B
I-10	B	B	Defect [b]	n/a [a]
I-11	B	B	B	n/a [a]

[a] Not applicable for this criterion
[b] Weld does not meet the criteria of the D level.

3.3 Fatigue test setup and measurements

Fatigue tests were conducted on the both box and I section specimens using a four-point bending test setup that enabled a uniform bending moment region in the middle of the beam structure (Fig 6). The fatigue load was established using a servo-hydraulic test rig that produced a 45–75 kNm maximum moment. The applied stress

*Corresponding author: antti.ahola@lut.fi (A. Ahola)

ratio was $R = 0.1$. The total rupture of the test specimen was the failure criterion in each fatigue test. In addition to uniform moment, the contacts of the four-point bending press cause local vertical forces at the beam's top flange which diminishes the fatigue durability within the press zone. This effect was taken into account when designing the cross-section geometries of test specimens (see the previous section).
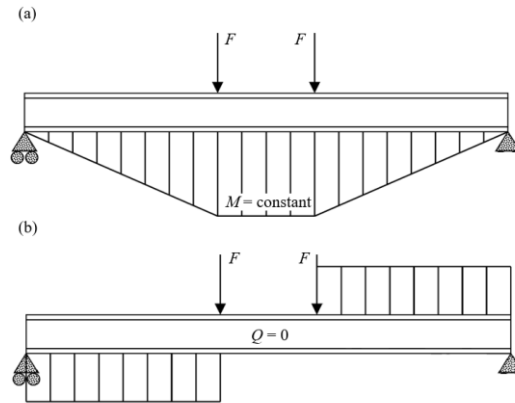
Fig 6. Two-dimensional (a) moment (M) and (b) shear (Q) diagrams of the four-point bending test. The applied cylinder force is $2F$.

The fatigue test setup for the box section specimens is depicted in Fig. 7. The stress range in the fatigue tests was measured using strain gauges. Fig. 7b-c present the strain gauge positioning at the bottom flanges of the box and I section specimens.
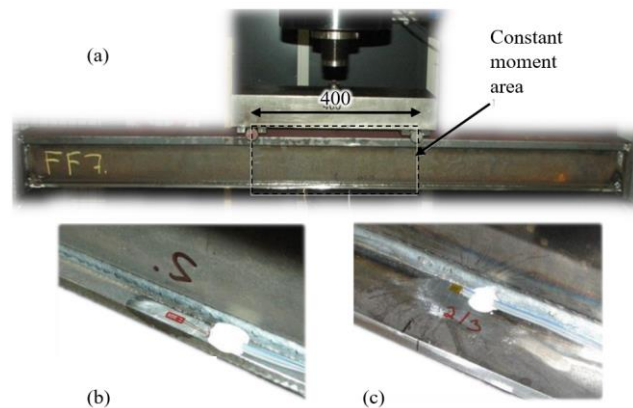
Fig 7. (a) Fatigue test set-up of the box girder specimens, and the instrumentation of the bottom flanges in (b) a box section specimen and (c) an I section specimen.

4 Results

4.1 Calculation of the stress ranges

The principles of stress determination are presented in Fig. 8. For the fatigue test analysis, stress range $\Delta\sigma_{str}$, determined based on the strain gage measurement, was used with a corresponding stress range at crack initiation

*Corresponding author: antti.ahola@lut.fi (A. Ahola)

location, i.e. maximum stress at the bottom flange $\Delta\sigma_{\max}$ was used for the fatigue failures occurring at the hot-rolled (HR) surface.

Fig. 8. Parameters for the analytical analysis of (a) bending and (b) shear stress in the studied beam structures. e is the distance from the neutral axis to the bottom surface of the flange, σ_w is the weld stress, $\sigma_{\max}$ is the maximum stress at the bottom surface of the flange, Q is the shear force, a_{eff} is the effective throat thickness and A is the cross-sectional area for calculating the first moment of area at the weld and $\overline{y}$ is the distance of area from the neutral axis.

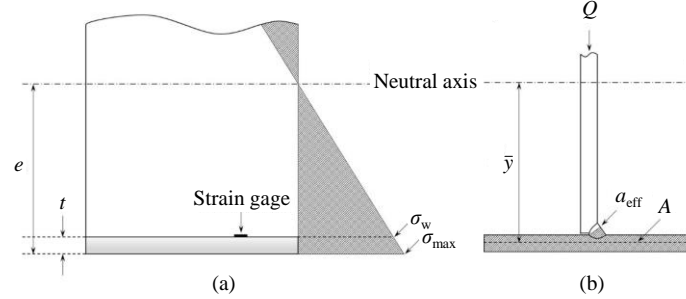The nominal stress at the weld ($\sigma_{w,\mathrm{nom}}$), calculated based on the second moment of area, and structural stress ($\sigma_{w,\mathrm{str}}$), calculated using strain gage measurements, which, in the case of fatigue fracture initiated from the weld joint between the web and flange, can be formulated as follows:

$$\sigma_{w,\mathrm{nom}} = \frac{M\left(e-t\right)}{I}, \tag{1}$$

$$\sigma_{w,\mathrm{str}} = \varepsilon E, \tag{2}$$

where M is the bending moment, t is the thickness of flange, I is the second moment of area, ε is the strain value measured by the strain gage, and E is Young's modulus.

If the fatigue fracture initiated from the base material at the bottom surface of the flange, the nominal ($\sigma_{\max,\mathrm{nom}}$) and structural ($\sigma_{\max,\mathrm{nom}}$) bending stresses are:

$$\sigma_{\max,\mathrm{nom}} = \frac{Me}{I}, \tag{3}$$

*Corresponding author: antti.ahola@lut.fi (A. Ahola)

$$\sigma_{\text{max,str}} = \sigma_w \left(1 + \frac{t}{e-t}\right) = \varepsilon E \left(1 + \frac{t}{e-t}\right). \tag{4}$$

The stress ranges calculated based on the strain gage measurements ($\sigma_{w,\text{str}}$ and $\sigma_{\text{max,str}}$) accounts for the geometrical imperfections present in the cross-section due to the manufacturing phase. However, the measurements indicated that the differences between the nominal stresses and structural stresses, i.e. Eq. (1) in comparison with Eq. (2), and Eq. (3) in comparison with Eq. (4), were less than 2%. If the fatigue fracture initiated from outside the uniform bending moment and zero-shear region (see Fig. 7a), the shear stress can be taken into account in the calculation of the weld stress:

$$\tau = \frac{QS}{Ia_{\text{eff}}}, \tag{5}$$

where S is the first moment of area ($S = A\overline{y}$), I is the second moment of area, and a_{eff} is the effective throat thickness (i.e. the thickness of a particular section of the cross-section at the point being measured), see also Fig. 8b.

This study followed the IIW recommendations [30] – thus, the nominal shear stress range was taken into account if it was more than 15% of the normal stress range and consequently, the maximum principal stress range was used due to the simultaneous in-phase variation of the normal and shear stresses.

4.2 Welded hollow sections

The stress ranges ($\Delta\sigma$) were based on the strain gage measurements, as well as the calculations presented in Section 4.1. In Table 6 and Table 7, the stress ranges correspond to the values acting at the location of fatigue failure ($\Delta\sigma_w$ in the case of failure originating from weld and $\Delta\sigma_{\text{max}}$ in the fatigue cracks initiated at the HR surface), and correspond to the values determined based on the strain gage measurements (Eq. (2) and Eq. (4)). In the box section specimens, $\Delta\sigma$ values were 347–422 MPa and the FAT classes of test specimens FF2 and FF3 were defined for the bottom flange as the FAT$_{\text{min}}$ value due to fatigue failures under the press rolls at the top flange (see Fig. 7a). Both these fatigue tests were terminated because fatigue cracks did not initiate in the bottom flange. Table 6 summarizes the results for each specimen.

Table 6. Fatigue test results for the box sections. N_f is the number of cycles to failure, and FAT$_{\text{mean}}$ is the mean fatigue strength (survival probability of $P_s = 50\%$) at two million cycles using an *S-N* curve slope parameter of $m = 3$.

*Corresponding author: antti.ahola@lut.fi (A. Ahola)

ID	Type	N_f [cycles]	$\Delta\sigma$ [MPa]	FAT$_{mean}$ [MPa]	Failure location
FF1	Single-sided, fillet	181822	347 [a]	156	Weld root – Outside the uniform moment area
FF2	Single-sided, fillet	217316	393	187	FAT$_{min}$ value, test interrupted
FF3	Single-sided, fillet	254471	376 [b]	189	FAT$_{min}$ value, test interrupted – Outside the uniform moment area
FF4	Single-sided, fillet	268889	394	202	Weld root
FF5	Single-sided, laser	182485	390	176	Weld toe
FF6	Single-sided, laser	179318	422 [a]	189	Weld toe – Near the line of the loading point
FF7	Single-sided, fillet	84493	390	136	Weld root
FF8	Single-sided, fillet	136169	388	158	Weld root

[a] Considered the shear stress range which was more than 15% of the normal stress range

[b] Not considered the shear stress range which was less than 15% of the normal stress range

4.3 Welded I sections

In the I section specimens, the $\Delta\sigma$ values were 387–655 MPa. The three reference I section specimens (I-1, I-2, I-3) with double-sided fully penetrating welds achieved a mean fatigue strength of FAT$_{mean}$ = 223 MPa (fixed m = 3) or 273 MPa (calculated $m \approx 3.9$). Table 7 summarizes the results of fatigue-tested welded I sections. In the I section with the penetration to thickness ratio of p/t = 0.75, the fatigue failures did not occur in the weld region but at the HR surfaces of the bottom flanges. Thus, those results are not directly comparable with the results in which the failure occurred in the weld region.

Table 7. Fatigue test result for the I sections. FAT$_{mean}$ is the mean fatigue strength (survival probability of P_s = 50%) at two million cycles using an S-N curve slope parameter of m = 3.

ID	Type	p/t	N_f [cycles]	$\Delta\sigma$ [MPa]	FAT$_{mean}$ [MPa]	Failure location
I-1	Double-sided, full penetration	–	275034	437	225	Bottom flange – HR surface
I-2	Double-sided, full penetration	–	184964	555	251	Bottom flange – HR surface
I-3	Double-sided, full penetration	–	53037	655	195	Bottom flange – HR surface
I-4	Single-sided, fillet	0.22	185930	425 [a]	192	Weld root – Near the line of the loading point
I-5	Single-sided, groove	0.75	243202	435	215	Bottom flange – HR surface
I-6	Single-sided, groove	0.86	253458	387 [a]	194	Weld imperf. – Near the line of the loading point
I-7	Single-sided, groove	0.68	199771	414 [a]	192	Weld root – Outside the uniform moment area
I-8	Single-sided, groove	0.63	201736	398	185	Weld root
I-9	Double-sided, fillet	–	127608	391	156	Weld imperf.
I-10	Single-sided, groove	2.31	67381	411	133	Weld defect
I-11	Single-sided, groove	1.04	119649	409 [a]	160	Weld imperf. – Near the line of the loading point

[a] Considered the shear stress range which was more than 15% of the normal stress range

4.4 Summary of the results

The fatigue test were divided into three main categories in accordance with the failure locations: from the HR surface, weld root and weld imperfection. The I sections with fully penetrating welds (IDs I-1, I-2, I-3) were chosen for as the reference (highest fatigue capacity) and those tests were carried out with three different stress

*Corresponding author: antti.ahola@lut.fi (A. Ahola)

ranges. This resulted in mean fatigue strength of 320 MPa (fixed $m = 5$, corresponding to the *S-N* curve of the base material) without fatigue failures in the weld area. Instead, in those specimens, fatigue failures occurred at the HR surface of the bottom flange. Fatigue performance of an I-beam (ID I-5) with optimal welding configuration was close to the reference series, with a similar crack initiation at the HR surface. The combined results are presented in Fig. 9. It can be seen that fatigue performance was affected by weld root quality and weld imperfections. In the case of high-quality welds, the HR surface limited the fatigue performance.

In comparison with the results of a prior study [24] on the re-evaluation of fatigue design categories (FAT150 for the mean fatigue strength of longitudinal welds without start/stop positions), it can be observed that the specimens failing from the weld toe and HR surface exceed the upper bound of fatigue design curve, and show thus higher fatigue strength than usually expected for these joints. Those specimens failing from weld root show the lowest fatigue strength in the tested series and correspond to the mean fatigue strength of the prior study [24].
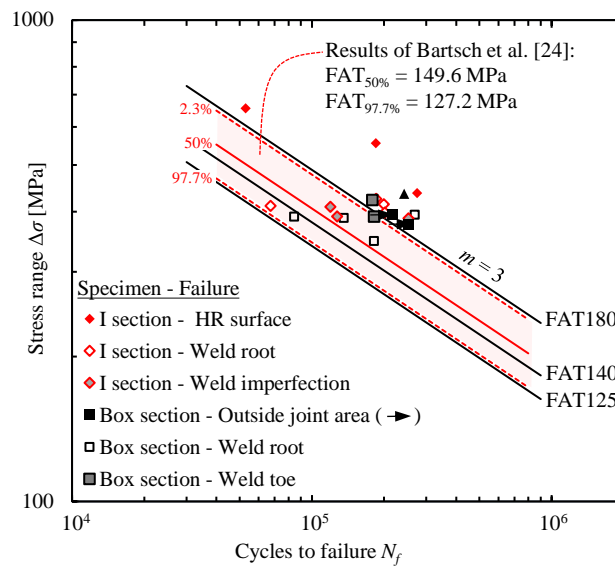
Figure 9. Fatigue test results and design *S-N* curves. Design curves in accordance with the fatigue class provided in Table 1, and the scatter bands of prior experimental results (longitudinal welds without start and stop positions) as per Bartsch et al. [24].

5 Discussion

The present study experimentally evaluated the fatigue strength of load-carrying longitudinal welds in beam structures (welded box and I sections) made of UHSS. The aim was to investigate the applicability of the current fatigue design codes and recommendations for assessing the fatigue strength of these welds. In comparison to the design *S-N* curves (see Table 1 and Fig. 9), the mean fatigue strength of the fatigue-tested beams was distinctly

*Corresponding author: antti.ahola@lut.fi (A. Ahola)

higher. For instance, a mean fatigue strength up to 223 MPa ($m = 3$) was found for the K-butt-welded I section beams. As expected, the non-existence of notch-like imperfections due to transverse discontinuities (e.g., the irregular geometry at the weld root) led to a high fatigue strength of the welded UHSS joints even though a higher material strength does not generally contribute to a higher fatigue strength in welded joints. In the case of fully penetrating single-sided welds with break-outs (Specimen ID I-10, see Fig. 5), the fatigue strength of longitudinal UHSS joints decreased significantly, as shown in Table 6 (Specimen ID I-10), and no major improvement in comparison with the design recommendations was found.

Fractography of the failed crack surfaces explains the obtained results, i.e. there are different fatigue failure modes in the joint area, as presented in Fig. 10. The failures at the joint regions initiated from imperfections and discontinuities; namely individual weld pores near the weld root (Fig. 10a) and at the weld metal (Fig. 10b); irregular shape/discontinuity at the weld root in the GMA-welded joint (Fig. 10c) and at the weld toe of the laser-welded joint (Fig. 10d). Fatigue strength is limited by the fatigue performance of the HR surface, and in the high-quality weldments, the fatigue failures occurred at the surface of the bottom flange (Fig. 10e–f). The fatigue strength of the longitudinal weldments was similar to that of the UHSS-grade cut edge details reported in [16]. Therefore, such welded details can potentially fail from the weld of the web-to-flange connection, and the cut edge of flange and web members.

(a) ID I-9 - double-sided fillet weld   (b) ID I-11 – single-sided groove weld   (c) ID FF-8 – single-sided fillet weld

(d) ID FF5 - single-sided laser weld   (e) ID I-2 - double-sided fillet weld (full penetration)   (f) ID I-5 - single-sided weld with groove
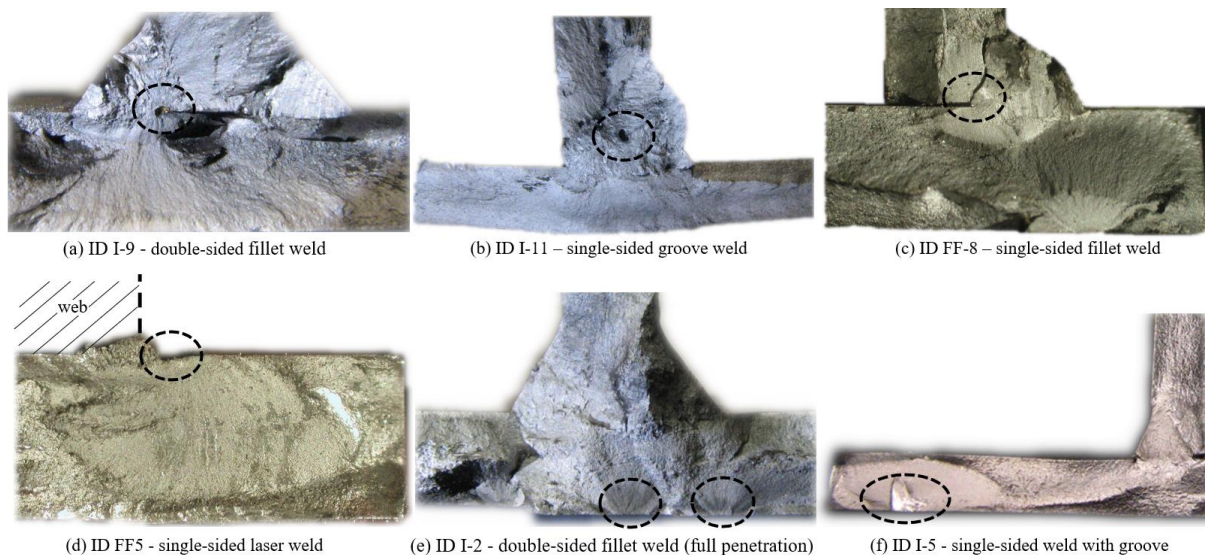
Fig. 10. The different fatigue failure modes and crack initiation locations of tested beams.

The fatigue performance of the tested longitudinal welds is comparable to the performance of the cut edges reported in [44]. For an ideal fatigue design, the fatigue performance of the cut edges and welded details should

*Corresponding author: antti.ahola@lut.fi (A. Ahola)

be identical. In this study, the fatigue cracks initiated mostly at the weld root and not at the edge of laser cut web member. Further studies on the relationship between the weld and the cut edge should be conducted for such web-to-flange connections and partial penetration welds. It is also worth mentioning that the fatigue performance of the base material failures found in this study (see Fig. 10e-f) was significantly lower than in the base material specimens with machined edges fatigue-tested in [45]. Residual stress measurements were not carried within this study, but a high tensile residual stress field induced by the welding, together with the size factor and scratches from handling the beams could have affected the fatigue capacity of the HR surface of the bottom flange.

As shown in Table 5, the welds were mainly categorized into the B level as per the EN ISO 5817 standard. The specimens FF-7–8 were in the C class (intermittent undercut) and defects was found in the specimen I-10 (excessive penetration, out of range in the D level). The excessive penetration can be regarded as detrimental in terms of fatigue performance since it does not usually provide a continuous profile and causes transverse discontinuities decreasing fatigue strength. The specimen I-10 also showed the lowest fatigue strength, FAT_{mean} = 133 MPa but was still above the design curve. The intermittent undercuts found in the specimens FF-7–8 can drastically decrease fatigue strength if the loading direction is perpendicular to weld. In the specimens, the fatigue failures occurred at the weld root showing that the undercuts were not critical locations in this load case. In general, as the EN ISO 5817 standard is mainly based on the imperfections and defects at the cross-sectional profile and good workmanship in welding, it does not necessarily provide correct quality criteria for the joints subjected to longitudinal cyclic loading. These observations highlight the need for careful consideration of quality criteria in accordance with the joint and loading type, also suggested in a study by Björk et al [46].

Crack initiation and propagation periods were not monitored during the fatigue tests (failures mainly occurred at the constant moment area, Fig. 7a). Fractography (see Fig. 10) and polished sections (Fig. 4 and Fig. 5), however, indicates that those specimens failing from individual pores and HR surface were free of crack-like notches and imperfections and, consequently, had a great share of crack initiation life. This observation also is supported by the fatigue test results; mean fatigue strengths exceeded the upper bound of prior experimental data, and were up to FAT_{mean} = 251 MPa in these specimens.

A closer look at the effects of the weld penetration to web thickness ratio (p/t) in the I section specimens, shown in Fig. 11, reveals that fillet welding and partial penetration in single-sided weldments led to higher fatigue strength than with fully penetrated welds. According to the findings of this study, the web should be positioned without an air gap to ensure a longitudinally continuous weld penetration and, therefore, high fatigue performance. Break-outs in single-sided welds significantly decrease the fatigue strength, as shown in Fig. 11. Cut edge

*Corresponding author: antti.ahola@lut.fi (A. Ahola)

perpendicularity and tack weld positions should be considered to ensure high weld quality. In general, fatigue performance is higher when using fewer passes in welding due to the increased risk of interpass defects and imperfections in multipass welding.
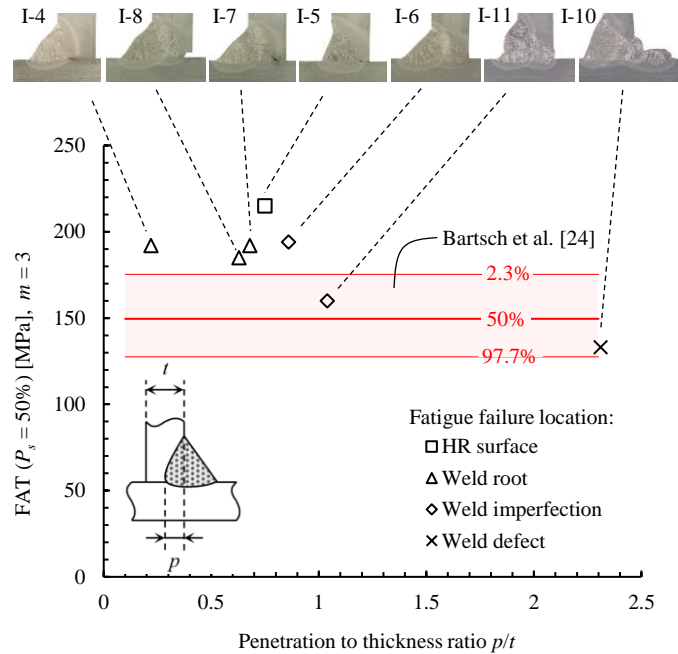

Fig. 11. Effect of penetration on the fatigue strength in the single-sided welded I section specimens.

Due to the limited number of test specimens in each joint configuration (weld and groove type were altered), only the fixed slope of $m = 3$ was used in this study to determine the fatigue strength of these joints as per the fatigue design recommendations [30,43]. Further studies should be carried out to obtain a free slope of these joints. The fatigue tests were performed at the intermediate life (< 300000 cycles), and further work should be conducted to evaluate the high-cycle fatigue performance of these joints. Nevertheless, the use of UHSS materials aims to increase static and cyclic stress levels, which highlights the importance of fatigue design criterion e.g. in bridge structures made of HSS and UHSS [47].

6 Conclusions

The present paper experimentally investigated the fatigue strength of longitudinal load-carrying welds in beam structures made of UHSS, focusing on single- and double-sided weldments in hollow and I sections. Based on the fatigue test results and subsequent analysis and fractography, the following conclusions can be drawn:

- The current design recommendations are slightly conservative for longitudinal load-carrying welds made of UHSS if the continuous weld profile at the weld surface and root is obtained. The lowest mean fatigue

*Corresponding author: antti.ahola@lut.fi (A. Ahola)

strength was 133 MPa ($m = 3$) for a fully penetrating single-sided weld with a break-out. For K-butt-welded I sections, the weld region was not even the fatigue-critical location of the beam component, and a mean fatigue strength up to 223 MPa ($m = 3$) was obtained for those specimens. Consequently, longitudinal UHSS components can obtain a higher fatigue strength than current fatigue design recommendations provide. According to this study, the characteristic design curve FAT140 ($m = 3$) can be used for both single- and double-sided welds with partial penetration and without start/stop positions in the S960 grade.

- Longitudinally continuous weld penetration, resulting from a non-fused root face with zero air gap in single- and double-sided longitudinal welds is of paramount importance: The root face of the web plate acts as a backing plate if the fit between the web and flange members is assured, and high fatigue strength is obtained regardless of the degree of weld penetration.

Acknowledgements

References

[1] O.-P. Hämäläinen, T. Björk, Optimization of the Cross-Section of a Beam Subjected to Bending Load, in: K. Jarmai, J. Farkas (Eds.), Proc. Int. Conf. Des. Fabr. Econ. Met. Struct., 2013: pp. 17–22. doi:10.1007/978-3-642-36691-8_3.

[2] F. Javidan, A. Heidarpour, X.-L. Zhao, J. Minkkinen, Application of high strength and ultra-high strength steel tubes in long hybrid compressive members: Experimental and numerical investigation, Thin-Walled Struct. 102 (2016) 273–285. doi:10.1016/j.tws.2016.02.002.

[3] M. Amraei, M. Dabiri, T. Björk, T. Skriko, Effects of workshop fabrication processes on the deformation capacity of S960 ultra-high strength steel, J. Manuf. Sci. Eng. 138 (2016) 121007. doi:10.1115/1.4033930.

[4] M. Amraei, A. Ahola, S. Afkhami, T. Björk, A. Heidarpour, X.-L. Zhao, Effects of heat input on the mechanical properties of butt-welded high and ultra-high strength steels, Eng. Struct. 198 (2019). doi:10.1016/j.engstruct.2019.109460.

[5] S. Afkhami, T. Björk, J. Larkiola, Weldability of cold-formed high strength and ultra-high strength steels, J. Constr. Steel Res. 158 (2019) 86–98. doi:10.1016/j.jcsr.2019.03.017.

[6] H.P. Lieurade, I. Huther, F. Lefebvre, Effect of weld quality and postweld improvement techniques on the fatigue resistance of extra high strength steels, Weld. World. 52 (2008) 106–115. doi:10.1007/BF03266658.

[*]Corresponding author: antti.ahola@lut.fi (A. Ahola)

[7]   C.M. Sonsino, Effect of residual stresses on the fatigue behaviour of welded joints depending on loading conditions and weld geometry, Int. J. Fatigue. 31 (2009) 88–101. doi:10.1016/j.ijfatigue.2008.02.015.

[8]   M. Braun, X. Wang, Fatigue strength improvement by weld toe grinding: a data review. IIW-document XIII-2861-2020, 2020.

[9]   T. Skriko, M. Ghafouri, T. Björk, Fatigue strength of TIG-dressed ultra-high-strength steel fillet weld joints at high stress ratio, Int. J. Fatigue. 94 (2017) 110–120. doi:10.1016/j.ijfatigue.2016.09.018.

[10]   J. Berg, N. Stranghöner, Fatigue behaviour of high frequency hammer peened ultra high strength steels, Int. J. Fatigue. 82 (2016) 35–48. doi:10.1016/j.ijfatigue.2015.08.012.

[11]   M. Leitner, M. Stoschka, W. Eichlseder, Fatigue enhancement of thin-walled, high-strength steel joints by high-frequency mechanical impact treatment, Weld. World. 58 (2014) 29–39. doi:10.1007/s40194-013-0097-4.

[12]   T. Skriko, T. Björk, T. Nykänen, Effects of weaving technique on the fatigue strength of transverse loaded fillet welds made of ultra-high-strength steel, Weld. World. 58 (2014) 377–387. doi:10.1007/s40194-014-0123-1.

[13]   P.J. Haagensen, S.J. Maddox, IIW Recommendations on Methods for Improving the Fatigue Strength of Welded Joints, Woodhead Publishing, 2013.

[14]   A. Ahola, T. Björk, Fatigue strength of misaligned non-load-carrying cruciform joints made of ultra-high-strength steel, J. Constr. Steel Res. 175 (2020) 106334. doi:10.1016/j.jcsr.2020.106334.

[15]   B. Möller, J. Baumgartner, R. Wagener, H. Kaufmann, T. Melz, Low cycle fatigue life assessment of welded high-strength structural steels based on nominal and local design concepts, Int. J. Fatigue. (2017). doi:10.1016/j.ijfatigue.2017.02.014.

[16]   M.J. Ottersböck, M. Leitner, M. Stoschka, W. Maurer, Crack initiation and propagation fatigue life of ultra high-strength steel butt joints, Appl. Sci. 9 (2019). doi:10.3390/app9214590.

[17]   A. Ahola, T. Skriko, T. Björk, Fatigue strength assessment of ultra-high-strength steel fillet weld joints using 4R method, J. Constr. Steel Res. 167 (2020) 105861. doi:10.1016/j.jcsr.2019.105861.

[18]   M. Stoschka, M. Leitner, G. Posch, W. Eichlseder, Effect of high-strength filler metals on the fatigue behaviour of butt joints, Weld. World. 57 (2012) 85–96. doi:10.1007/s40194-012-0010-6.

[19]   H. Jiao, F. Mashiri, X.L. Zhao, Fatigue behavior of very high strength (VHS) circular steel tube to plate T-joints under in-plane bending, Thin-Walled Struct. 68 (2013) 106–112. doi:10.1016/j.tws.2013.03.006.

[20]   A. de Castro e Sousa, A. Nussbaumer, Multiaxial ultra low cycle fatigue in welded high strength steel structural components, J. Constr. Steel Res. 153 (2019) 473–482. doi:10.1016/j.jcsr.2018.10.028.

[21]   Y. Wu, W. Li, Q. Lan, Fatigue life prediction of welded box girder structures, Adv. Mech. Eng. 9 (2017) 1–10. doi:10.1177/1687814017728838.

[22]   T. Björk, A. Ahola, T. Skriko, On the distortion and warping of cantilever beams with hollow section, Weld. World. 64 (2020) 1269–1278. doi:10.1007/s40194-020-00911-5.

[23]   M. Feldmann, H. Bartsch, U. Kuhlmann, K. Drebenstedt, T. Ummenhofer, B. Seyfried, Auswertung von Ermüdungsversuchsdaten zur überprüfung von Kerbfallklassen nach EC3-1-9, Stahlbau. 88 (2019) 1004–1017. doi:10.1002/stab.201900066.

[24]   H. Bartsch, K. Drebenstedt, B. Seyfried, M. Feldmann, U. Kuhlmann, T. Ummenhofer, Analysis of fatigue test data to reassess EN 1993-1-9 detail categories, Steel Constr. 13 (2020). doi:10.1002/stco.202000019.

[25]   EN 1993-1-9, Eurocode 3: Design of steel structures - Part 1-9: Fatigue, 2005.

[*]Corresponding author: antti.ahola@lut.fi (A. Ahola)

[26] J. Fisher, K. Frank, M. Hirt, B. McNamee, Effect of weldments on the fatigue strength of steel beams, 1969.

[27] D. Böhme, R. Helwig, R. Olivier, W. Ritter, Einfluß von Poren aus Fertigungsbeschichtungen auf die Schwingfestigkeit längsbeanspruchter Kehlnähte (in German), Schweißen Und Scheiden. 35 (1983) 308–312.

[28] T. Hanji, K. Tateishi, M. Shimizu, D. Uchida, K. Asano, R. Kimura, Fatigue strength of cruciform joints and longitudinal joints with laser-arc hybrid welding, Weld. World. 63 (2019) 1379–1390. doi:10.1007/s40194-019-00745-w.

[29] DNVGL-RP-C203, Fatigue Design of Offshore Steel Structures, 2016.

[30] A. Hobbacher, Recommendations for Fatigue Design of Welded Joints and Components, 2nd ed., Springer International Publishing, Cham, 2016.

[31] EN 13001-3-1, Cranes. General Design. Part 3-1: Limit States and proof competence of steel structure, 2018.

[32] EN 1993-1-8, Eurocode 3: Design of steel structures - Part 1-8: Design of joints, 2005.

[33] E. Niemi, Design of Plate Structures (in Finnish). Tekninen tiedotus 2, 2003, Teknologiateollisuus, Helsinki, 2003.

[34] EN ISO 5817, Welding. Fusion-welded joints in steel, nickel, titanium and their alloys (beam welding excluded). Quality levels for imperfections., 2014.

[35] T. Skriko, Dependence of manufacturing parameters on the performance quality of welded joints made of direct quenched ultra-high-strength steel. Doctoral Dissertation, Lappeenranta University of Technology, Lappeenranta University of Technology, 2018.

[36] D. Rademacher, Zur sicheren Anwendung feuerverzinkter Bauteile im Stahl- und Verbundbrückenbau (in German). Doctoral dissertation, Technishe Universität Dortmund, 2017.

[37] J. Kömi, P. Karjalainen, D. Porter, Direct-Quenched Structural Steels, in: R. Colás, G.E. Totten (Eds.), Encycl. Iron, Steel Their Alloy., CRC Press, Boca Raton, 2016: pp. 1109–1125.

[38] T. Björk, J. Toivonen, T. Nykänen, Capacity of fillet welded joints made of ultra high-strength steel, Weld. World. 56 (2012) 71–84. doi:10.1007/BF03321337.

[39] T. Björk, A. Ahola, N. Tuominen, On the design of fillet welds made of ultra-high strength steel, Weld. World. 62 (2018) 985–995. doi:10.1007/s40194-018-0624-4.

[40] SSAB, Data sheet for Strenx 960 MC, (2020). https://www.ssab.com/products/brands/strenx/products/strenx-960-mc (accessed October 23, 2020).

[41] Voestalpine Böhler Welding, Data sheet for Union X96. Datasheet: Union X 96, (2020). www.vabw-service.com/documents/boehler/datenblaetter/en/T_Union X 96_de_en_5.pdf?cache=1603353793 (accessed October 23, 2020).

[42] EN 10025-2, Hot rolled products of structural steels - Part 2: Technical delivery conditions for non-alloy structural steels, 2004.

[43] EN 1993-1-1, Eurocode 3: Design of steel structures - Part 1-1: General rules and rules for buildings, 2005.

[44] K. Lipiäinen, A. Ahola, T. Skriko, T. Björk, Fatigue strength characterization of high and ultra-high-strength steel cut edges. Revision submitted, Eng. Struct. (2020).

[*]Corresponding author: antti.ahola@lut.fi (A. Ahola)

[45]   J.O. Sperle, Influence of parent metal strength on the fatigue strength of parent material with machined and thermally cut edges, Weld. World. 52 (2008) 79–92. doi:10.1007/BF03266656.

[46]   T. Björk, J. Samuelsson, G. Marquis, The need for a weld quality system for fatigue loaded structures, Weld. World. 52 (2008) 34–46. doi:10.1007/BF03266615.

[47]   O. Skoglund, J. Leander, R. Karoumi, Overview of Steel Bridges Containing High Strength Steel, Int. J. Steel Struct. (2020). doi:10.1007/s13296-020-00360-2.

[*]Corresponding author: antti.ahola@lut.fi (A. Ahola)

Appendix A. Welding parameters of the test specimens

Table A.1. Welding parameters of the box and I section specimens.

Specimen type	Welding process	Pass	Pos.	I [A]	U [V]	v_{wire} [m/min]	v_{travel} [mm/s]	θ_{travel} [°]	θ_{tilt} [°]	CTWD [mm]	Q [kJ/mm]
Box section	*GMAW*										
	multi-pass	Root	PB	215–285	25.8–26.4	14.0–14.1	6.5–8.3	0–30[a]	45	15 - 20	0.55–0.90
		Fill	PB	215–290	25.8–26.4	13.2–14.1	6.5–8.3	0–30[a]	45	15 - 20	0.55–0.92
		Cap	PB	215–255	26.1–26.4	8.0	8.3	0–30[a]	45	15 - 20	0.55–0.64
	single-pass		PB	215–290	26.4–26.6	9.1	12.0–13.5	30[a]	45	15 - 20	0.38–0.46
	Laser										
	single-pass		PB	Laser power P = 5 kW			30.0–33.0	0	15–20	-	0.14–0.15
I section	*GMAW*										
	multi-pass	Root	PA[b]/PB	180[b]–231	22.1[b]–25.3	9.0[b]–10.0	2.0[b]–7.0	5–10[a]	0[b]–35	18–20	0.53[c]–1.59[b]
		Fill	PA[b]/PB	205[b]–206	26.5[b]–26.6	10.0–10.5[b]	4.7[b]–7.0	5[a]	0[b]–35	18–20	0.55[c]–0.92[b]
		Cap	PA[b]/PB	212–225[a]	26.0–27.9[b]	10.0–11.0[b]	3.6[b]–7.0	5–10[a]	0[b]–35	18–20	0.55[c] 1.40[b]
	single-pass	Fillet	PB	223–227	27.0–27.2	10.5	5.8	10[a]	35	18	0.73–0.75[c]
		Groove	PB	229–264	24.1–26.5	10.5–10.6	5.3–5.8	10–13[a]	35	16–18	0.73–0.84[c]

I is the welding current, U is the welding voltage, v_{wire} is the wire feed rate, v_{travel} is the travel speed of the welding torch, θ_{travel} is the travel angle of the welding torch (pushing/pulling), θ_{tilt} is the tilt angle of the welding torch, CTWD is the contact tip to work distance, and Q is the heat input.

[a] Forehand technique (pushing)

[b] Manual welding

[c] Considered the electrical cable resistance of the robot welding equipment

*Corresponding author: antti.ahola@lut.fi (A. Ahola)